ISSN No:-2456-2165

Helical Transport in Nanowires with Rashba Spin-Orbit Coupling

[1]Effiong E. Eyibio, [2]Eno E. Ituen, [3]Monday Etiufan Udoh [4]Jude Odams Gian

[1]Department of Physics, University of Uyo, Nigeria

Abstract:- Two nanowires coupled together such that one has only spin-orbit coupling and the other have Spin-orbit coupling and magnetism; reflection, and transmission of an electron occurs their interface. In the absence of the barrier strength z, reflection would not be possible and the electron will be maximally transmitted. However, when the chemical potential in the right region was greater than that of the left region, it acted as a small barrier, and allowed for small reflection at low energy. This reflection became insignificant at higher energy. Transmission of an electron reduced as z increased while reflection increased, but as the energy of the electron increased, transmission increased while reflection reduced to minimal. In the N1-N2-N3 junctions, N2 acts as a barrier and causes spin-up reflection even when z = 0. On introducing the barrier z, N2-induced spin-up reflection occurs but reduces to minimum value as the energy of the electron increases, and then a barrier-induced spin-up reflection occurs, and keeps increasing to a steady value. During the second stage of spin-up reflection, increasing the energy energizes the reflection process. The tunneling conductance decreased with increasing barrier strength in both trivial and non-trivial phases. In the N1-N2-N3 junctions, when the length of the central wire, L = 1.0, the tunneling conductance could quickly attain maximum values as the energy of the electron increased in both phases unlike when L = 0. The zero-bias conductance abruptly jumped from G (0) = 0 in the trivial regime to G (0) = 1 in the non-trivial regime.

Keywords:- *Nanowire, Spin, Helical, Eigenvalues, Hamiltonian and Chemical potential.*

I. INTRODUCTION

In the last few years, most investigation on semiconductor nanowires (NWs) with Rashba spin-orbit coupling (RSOC) has centered on searching for Majorana quasi-particles, which are the building block for topologically secured quantum information [1-3]. When a Rashba NW is subjected to an external magnetic field, the wire is anticipated to have helical gap, and when such a system is in proximity to an s-wave superconductor, a single Majorana bound state at each end appears [1-2, 4]. Although signatures consistent with these extraordinary quasi-particles have been found in NWs proximized by superconducting films [5], the race to the demonstration of Majorana states have obstructed other inquisitively conceivable outcomes of NWs in quantum technologies.

Without a question, NWs coming to lengths of distinctive μm and appearing quantum coherent transport are these days made both within the clean ballistic [6-9] and are realized in suspended geometries [10], in arrays [11-12] and networks [11]. Additionally, they can be utilized as adaptable substrates for hybrid epitaxial improvement on chosen angles to design heterostructures with ferromagnets and superconductors [13]. As well, NWs are an incredibly adaptable and tunable platform for nano-electronics since their conduction properties can be controlled both magnetically, for example, by applying a parallel magnetic field along the NW center and hence opening up a gap within the spectrum, or electrically by controlling the RSOC through gate voltages [14-16].

A vital necessity for the appearance of Majorana modes is the opening of a gap within the range at the Dirac point due to an applied external magnetic field. Without a doubt, the creation of such a gap can be understood most effortlessly for non-interacting electrons, and the fate of this "helical gap" within the interacting situation has been considered in recent years utilizing renormalization group (RG), Wigner crystal hypothesis and numerical simulations [17-20]. In fact, an applied external magnetic field breaks time-reversal symmetry. Notwithstanding, without external magnetic field when the system is time-reversal symmetric, it is reliable to permit for another spin non-conserving process - spin-umklapp scattering, which can moreover open a partial gap close to the band crossing [29]. Whereas this sort of scattering has been anticipated based on symmetry contentions, much less consideration has been given to understanding the microscopic mechanism behind it [4, 21-22].

In principle, in an interacting quasi-1D Rashba wire, helical gaps can be created by either a magnetic field or by spin-umklapp scattering. This prompts the question around whether the two conceivable basic causes can be recognized experimentally. Each of these processes lead to exceptionally comparative experimental signatures in conductance values, where the opening of a helical gap comes about in a splitting of the conductance into half as the chemical potential is tuned near to the Dirac point [23].

ISSN No:-2456-2165

Realizing and controlling Majorana fermions (MFs) in wires may be unequivocally less complex; [2] have shown analytically that nanowires with strong spin-orbit coupling, e.g., InAs or InSb wires, frame a helical gap, associated with topological insulator edges. Subsequently, these wires bolster MF states when in the vicinity to s-wave superconductors, and a magnetic field. It has been numerically shown by [24], that the conductance in Nanowire-normal metal and normal metal-Nanowire-normal metal junctions exhibit helical gaps. The Nanowire contains SOC and magnetism, while the normal metal can contain SOC but no magnetism. Although [24] have numerically performed this calculation, it would be very interesting to obtain analytical expressions for the conductance following a wave-matching approach for a similar system. Therefore, this study aims at studying analytically helical transport in nanowires with Rashba spin-orbit coupling and magnetic field.

Our results show that when two nanowires are coupled such that the left region is a Rashba nanowire and the right region is a Rashba nanowire subjected to an external magnetic field perpendicular to SOC, electrons are reflected and transmitted uniquely at their interface; in the absence of any barrier z, the reflection will not occur although the chemical potential in the right region, μ_2 acts as a small barrier and allows for small reflection at low energy provided $\mu_2 > \mu_1$. This reflection becomes negligible at higher energies. The tunneling conductance decreases with increasing barrier strength in both the trivial and helical phases. In a two-junction system, N1–N2–N3, N2 acts as a barrier and causes N2- induced spin-up reflection at z = 0. N2-induced spin-up reflection reduces to a minimum when z is introduced and as the energy of the electron increases, hence barrier–induced reflection will occur and keep increasing to a steady value. Also, when L = 1, the tunneling conductance will quickly attain maximum value as the energy of the electron increases in both phases unlike the case of a short junction. The zero-bias conductance abruptly jumps from $ G (0) = 0 in the trivial region to G (0) = 1 in the helical phase.

The paper is organized as follows. In Section 2, we model a system of two nanowires; one containing only SOC and the other containing SOC and magnetism. We will also discuss the scattering states at the junction of the two wires, hereby obtaining the reflection and transmission probabilities and the normal conductance. In Section 3, we will demonstrate a model for two junctions containing a normal metal, intertwined between two nanowires and then obtain the Reflection and Transmission probabilities and also the conductance. Finally, we will conclude our findings in Section 4.

II. MODEL

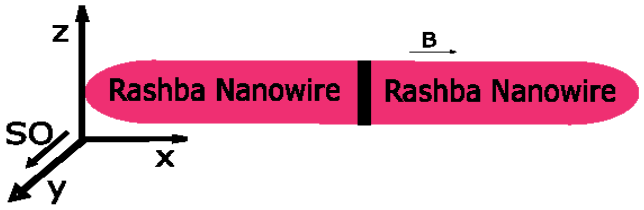

Fig 1 A Nanowire with Rashba SOC (In the Y-Direction) Having a Chemical Potential μ_1 and Coupled with Another Rashba Nanowire Having a Chemical Potential μ_2 Subjected to an External Magnetic Field.

Consider two nanowires, N1 and N2, which are coupled together such that N1 is a Rashba nanowire with chemical potential μ_1 and N2 is a Rashba nanowire with chemical potential μ_2 subjected to an external magnetic field. We have assumed a Rashba nanowire to be a nanowire containing SOC. The Hamiltonian of the two nanowires read [24]

$$H_0^s = \left(\frac{p^2}{2m} - \mu_s\right)\sigma_0 - \frac{\alpha_R}{\hbar} p\sigma_y + B_x\sigma_x, \quad [1]$$

where α_R is the Rashba spin-orbit coupling term and σ is the Pauli matrices, B is the applied magnetic field and s = 1, 2 with $B_1 = 0$, $B_2 = B$. The eigenvalues obtained from the characteristic equation are given by

$$E_{\pm}^s = \frac{\hbar^2 k_s^2}{2m} - \mu_s \pm \sqrt{(\alpha_s k_s)^2 + B_s^2}, \quad [2]$$

Where

$$k_s = \pm\sqrt{\frac{2m}{\hbar^2}}\sqrt{\mathrm{m}\alpha_R^2 + \mu_s + E_s \pm \sqrt{\frac{m^2\alpha_R^4}{\hbar^4} + \frac{2\mathrm{m}\alpha_R^2 E_s}{\hbar^2} + \frac{2\mathrm{m}\alpha_R^2\mu_s}{\hbar^2} + B_s^2}} \quad [3]$$

The normalized eigenfunctions obtained from the characteristic equation are $\psi_s(x) = \frac{1}{\sqrt{2}}\begin{pmatrix}\pm\gamma_s \\ 1\end{pmatrix} e^{ik_s^{\pm}x}$ and $\gamma = \frac{i\alpha_R k_s + B_s}{\sqrt{(\alpha_R k_s)^2 + B_s^2}}$. The plot of the energy eigenvalues obtained in Eq. (2) for N1 is shown in Fig. 2(a). Introducing spin-orbit coupling aligned along the y-axis shifts the two parabolas at k = 0 by momenta $\pm k_{SO} = \pm\frac{m\alpha_R}{\hbar^2}$ and by energy $\Delta E_{SO} = \pm\frac{m\alpha_R^2}{\hbar^2}$. There is no possibility to have a topological phase here when superconductivity is applied since for any μ there are two pairs of Fermi points that correspond to an even number and thus a trivial phase. Whereas, for a wire with a certain chemical potential and with no SOC, the energy versus momentum dispersion for a free electron consists of a single parabola. At k = 0, the electron has the minimum energy, $E_1 = -\mu_1$. As μ_1 increases, the energy reduces to the point where there is no Fermi points (See Appendix A for detail).

ISSN No:-2456-2165

Fig. 2(b) shows the energy spectrum of Eq. (2) for N2. The spectrum in this case has local and global extremes k = 0 with energy $-\mu \pm B$ and $\pm k_{\min} = \pm\sqrt{k_{SO}^2 - \frac{k_z^2}{4k_{SO}^2}}$ with energy $E_{\min} = -\mu - E_{SO} - \frac{B^2}{4E_{SO}}$. An applied external field perpendicular to the SOC lifts the spin degeneracy at k = 0 by removing the level crossing and opening a gap in the spectrum of 2B, this gap is known as the helical gap. When the system hosts an odd number of pairs of Fermi points per energy, the nanowire behaves as spinless. The system reaches the topological superconducting phase by placing the nanowire on an s-wave superconductor. When the chemical potential lies within this anti-crossing gap, the system has two Fermi points as opposed to four Fermi points in the case without an external magnetic field.

➢ *Scattering States*

The scattering states was obtained by considering the interface between the nanowires, N1, and N2, by connecting the wave functions in both regions at x = 0, reflection and transmission will occur. A right-moving spin-up electron from the left region can either be reflected as a spin-up and spin-down or transmitted as a spin-up and spin-down electron (See detailed derivation in Appendix B).

The probability of a reflection from spin-up to spin-up $R_{\uparrow\uparrow}$, reflection from spin-up to spin-down $R_{\uparrow\downarrow}$, transmission from spin-up to spin-up $T_{\uparrow\uparrow}$, and transmission from spin-up to spin-down $T_{\uparrow\downarrow}$ are given by

$$R_{\uparrow\uparrow} = |a|^2 \qquad R_{\uparrow\downarrow} = |b|^2$$
$$T_{\uparrow\uparrow} = \left|\frac{k_2^+ + \alpha}{k_1^+ + \alpha}\right| |c|^2 \qquad T_{\uparrow\downarrow} = \left|\frac{k_2^- - \alpha}{k_1^+ - \alpha}\right| |d|^2 \quad [4]$$

The coefficients; a, b, c and d are shown in Appendix B.

Reflection and transmission occurs at the interface uniquely (See Fig. 3), in absence of barrier z; reflection is insignificant and its value decreases with increasing E, at the same time electron is maximally transmitted; $T_{\uparrow\uparrow}$ increases with increasing E and decreases with increasing B while $T_{\uparrow\downarrow}$ increases with increasing B and decreases with increasing E. Also, as the barrier is increased, reflection is possible, from spin-up to spin-up, and insignificant from spin-up to spin-down electron. $R_{\uparrow\uparrow}$decreases as E increases because more energy is given to the electron to be transmitted, thereby reduce the reflection.

Figure 4 shows the variation of transmission and reflection probabilities with barrier strength, z. Like previously established, reflection increases as z increases but reduces as the energy of the system increases. We also noticed that spin-down reflection is not possible irrespective of the values of z and E. Transmission increases as the energy of the system increases, but the presence of a barrier reduces the transmission.

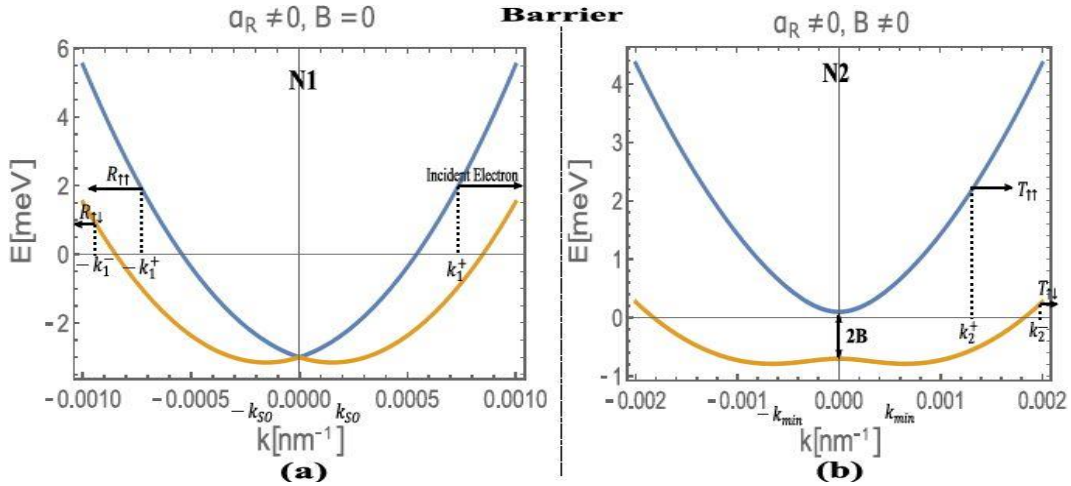

Fig 2 Energy Versus Wavevector, Showing Spin-Up Electron Travelling to the Right from the Left Region. The Electron can be Reflected as Spin-Up Electron at $-K_1^+$ and Spin-Down Electron At $-K_1^-$ or Transmitted as Spin-Up Electron At K_2^+ and Spin-Down Electron At K_2^-. The Values Correspond to Insb Nanowire [28]: M = 0.015m_e, $A_R = 20$mevnm and M = 0.03mev.

➢ *Conductance*

The physical assumption used to define the problem of normal conductance is that the distribution function of all incoming particles is given by the equilibrium Fermi function. Within the BTK (Blonder, Tinkham, and Klapwijk) [25], all incoming electrons from the N2 side have the distribution function $f_0(E)$, while those coming in from the N1 side are described by $f_0(E - eV)$.

Since the current must be conserved, it can be calculated in any plane. It is particularly convenient to do so in the N1 side of the interface where all current is carried by single particles. To find the current in our 1D model, we take the difference between $f_{\rightarrow}(E)$ and $f_{\leftarrow}(E)$; the distribution functions at the incident point and reflection point, and integrate over E. That is

$$I = QJ$$
$$= 2N(0)eV_F Q \int_{-\infty}^{\infty}[f_{\rightarrow}(E) - f_{\leftarrow}(E)]dE \quad [5]$$

where Q is an effective-neck cross-sectional area, including a numerical factor for angular averaging which will depend on the actual 3D geometry. For example, in the

ISSN No:-2456-2165

orifice model of point contact, $Q = \frac{\pi a^2}{4}$, where a is the radius of the orifice [26]. $N(0)$refers to the one-spin density of states at E_F.

Using the assumption of incoming populations, we have that

$$f_{\rightarrow}(E) = f_0(E - eV) \quad [6]$$

While

$$f_{\leftarrow}(E) = |a(E)|^2 f_{\rightarrow}(E) + |b(E)|^2 f_{\rightarrow}(E) + |c(E)|^2 f_0(E) + |d(E)|^2 f_0(E) \quad [7]$$

Therefore,

$$f_{\rightarrow}(E) - f_{\leftarrow}(E) = f_0(E - eV) - |a(E)|^2 f_0(E - eV) + |b(E)|^2 f_0(E - eV) + (|c(E)|^2 + |d(E)|^2) f_0(E)$$
$$= \big(f_0(E - eV) - f_0(E)\big)(1 - |a(E)|^2 - |b(E)|^2) \quad [8]$$

In obtaining Eq. (8), we used the properties $|a(E)|^2 + |b(E)|^2 + |c(E)|^2 + |d(E)|^2 = 1$. The quantity $(1 - |a(E)|^2 - |b(E)|^2)$ in Eq. (8) can be referred to as the transmission coefficient for electrical current. Therefore, Eq. (5) becomes

$$G(E) = G_0(1 - |a(E)|^2 - |b(E)|^2) \quad [9]$$

where $G_0 = \frac{e^2}{\hbar}$ is the normal state conductance for a quantum point contact and $G(E) = \frac{dI}{dV}$ is the zero-temperature differential conductance.

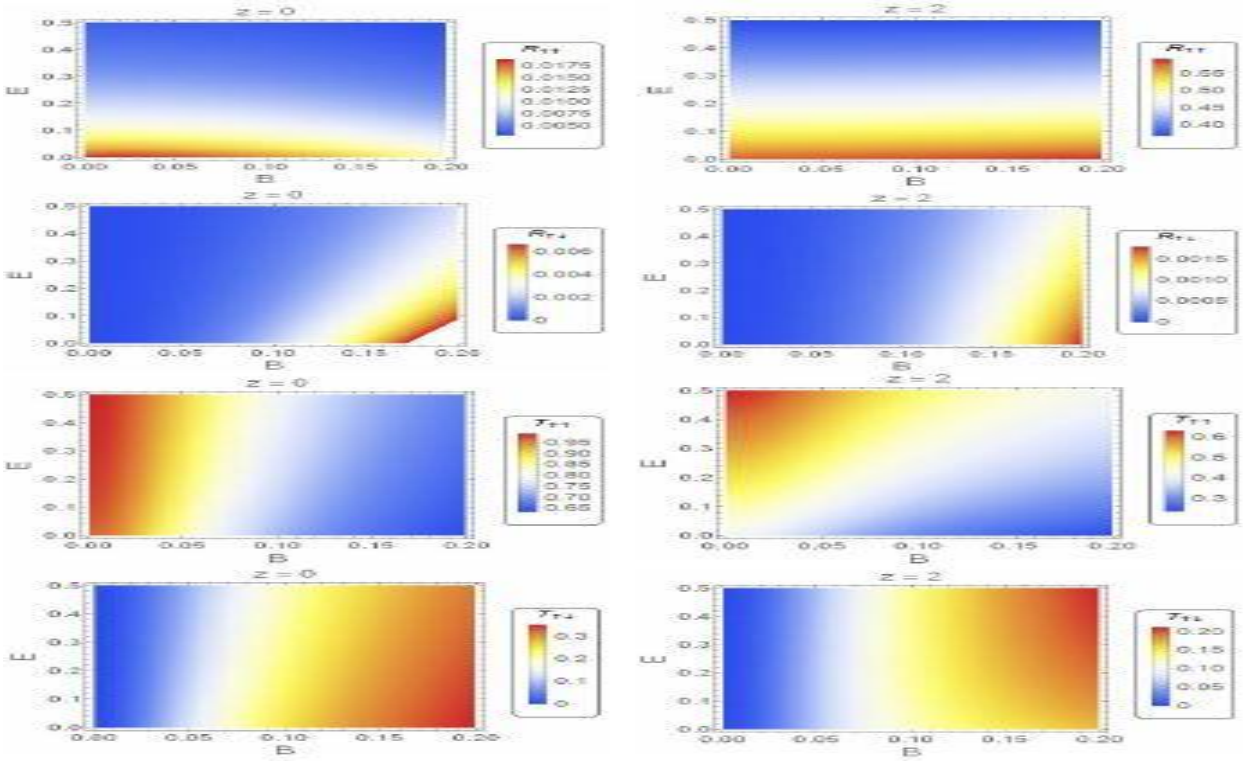

Fig 3 Intensity Plots of Transmission (T) and Reflection (R) Probabilities as Functions of the Incident Energy E and Magnetic Field B for Fixed Z. The Potential Barrier are Z = 0 And 2.0. The other Parameters are $\mu_1 = 0.2$, $\mu_2 = 0.5$ and $\alpha_R = 0.05$.

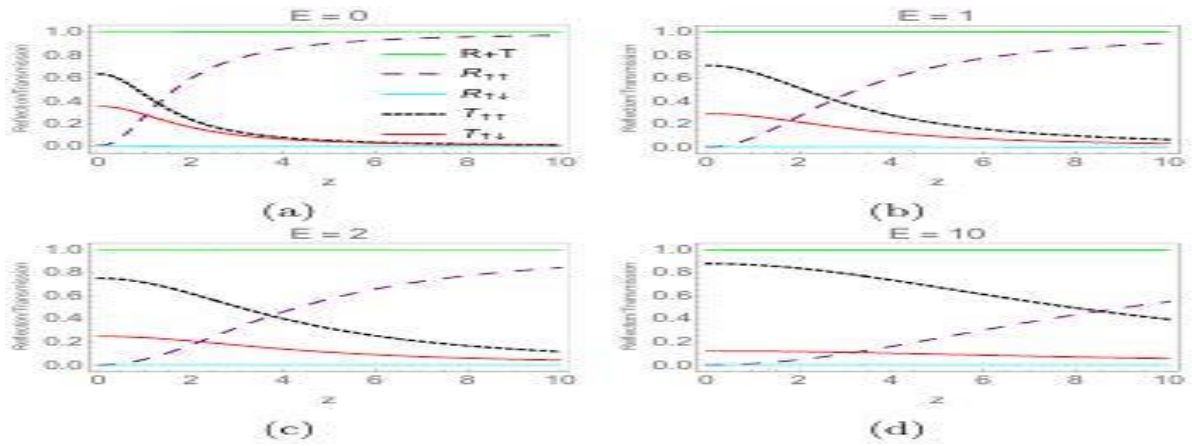

Fig 4 Transmission (T) and Reflection (R) Probabilities as Function of Z for Nanowire-Nanowire Junction. The Following Parameters were used: $\mu_1 = 0.2$, $\mu_2 = 0.5$, $\alpha_R = 0.05$ and B = 0.2.

The characteristic plots of the conductance as a function of the energy are shown in Fig. 5. The tunneling conductance G (E) decreases with increasing barrier strength z in both the trivial and helical phases. We also find that the zero-bias conductance abruptly jumps from G(0) = 0 in the trivial regime to G(0) = 1 in the helical regime. This is unlike what would be obtained in the superconducting state, where the electron can undergo the Andreev reflection, which effectively carries over 2 electrons to a superconductor. As such, a particle with energy E gets completely Andreev reflected, and G(E)/G_0(E) = 2 [27].

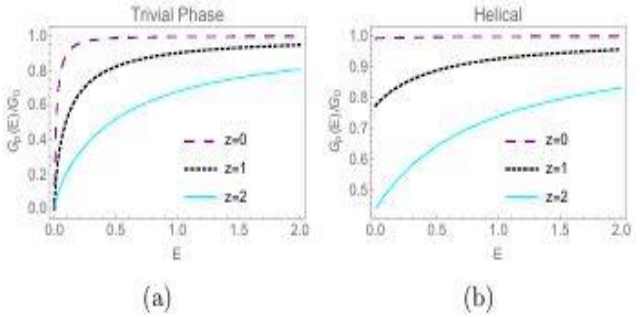

Fig 5 Variation of the Conductance G(E) with Energy E and Barrier Strength z for N1-N2 Junction. (a) Trivial Phase: $\mu_1 = 0$, $\mu_2 = 0.2$, $\alpha_R = 0.1$ and B = 0. (b) Helical: $\mu_1 = 0.4$, $\mu_2 = 0.5$, $\alpha_R = 0.1$ and B = 0.1.

III. NANOWIRE – NORMAL METAL – NANOWIRE JUNCTION (N1-N2-N3)

Consider a system of two junctions; nanowire – normal metal junction and normal metal - nanowire junction. The nanowires contain spin-orbit coupling only but no magnetism while the normal metal contains spin-orbit coupling and is subjected to an external magnetic field. N1 and N3 will represent Rashba nanowires, and N2 is the Rashba normal metal.

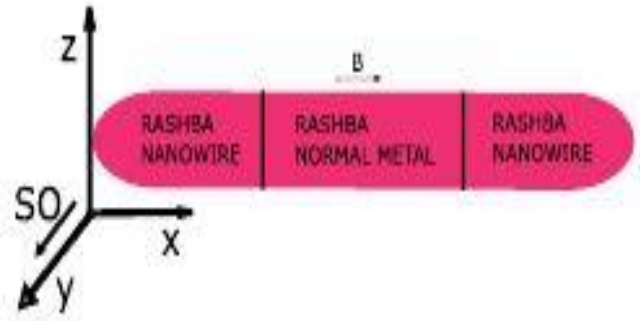

Fig 6 Two Junctions System Nanowire – Normal Metal Junction and Normal Metal – Nanowire Junction.

The Hamiltonians, eigenvalues, and eigenfunctions of each of the wires have been discussed in Section II. The scattering states will be obtained by first considering the interface between the Rashba nanowire N1, and normal metal N2, by connecting the wave functions in both regions at x = 0, reflection and transmission will occur (See the systematic diagram in Fig. 7). A right-moving spin-up electron from N1 can either be reflected as a spin-up and spin-down back to N1 or transmitted as a spin-up and spin-down electron to N2. Secondly, we consider the interface between the normal metal N2, and Rashba nanowire N3, by connecting the wavefunctions in both regions at x = L. The transmitted spin-up and spin-down electron in N2 become the incident electron at the interface x = L, the electron can also be reflected as a spin-up and spin-down electron back to N2 or transmitted as a spin-up and spin-down electron to N3.

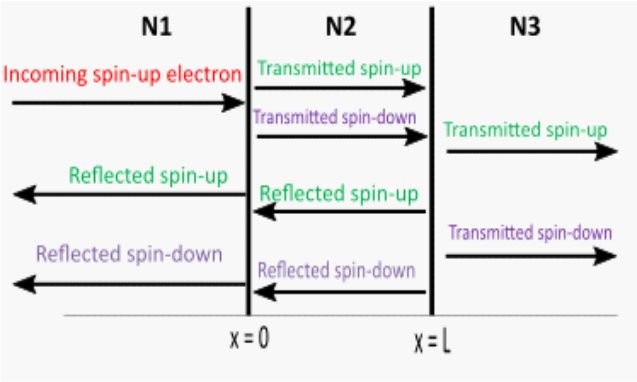

Fig 7 Systematic Diagram Showing Reflection and Transmission at the Two Junctions. The Junction N1-N2 is Located at X = 0 and the Junction N2-N3 Is Located at X = L.

The wavefunction describing the scattering states

$$\Psi(x) = \phi_1^+ e^{ik_1^+ x} + a_1\phi_1^+ e^{-ik_1^+ x} + b_1 e^{-ik_1^- x} \qquad x < 0$$
$$\Psi(x) = e_1\phi_2^+ e^{ik_2^+ x} + e\phi_2^- e^{ik_2^- x} + e_3\phi_2^+ e^{-ik_2^+ x} + e\phi_2^- e^{-ik_2^- x} \qquad 0 < x < L$$
$$\Psi(x) = c_1\phi_3^+ e^{ik_3^+ x} + d_1\phi_3^- e^{ik_3^+ x} \qquad x > 0$$

[10]

a_1, b_1, e_1, e_2, e_3, e_4, c_1 and d_1 are the coefficients of spin-up reflection in N1, spin-down reflection in N1, spin-up transmission into N2, spin-down transmission into N2, spin-up reflection into N2, spin-down reflection into N2, spin-up transmission into N3, and spin-down transmission into N3, respectively.

The respective probabilities are

$$R_{\uparrow\uparrow} = |a|^2, \qquad R_{\uparrow\downarrow} = |b|^2,$$
$$T_{\uparrow\uparrow} = \left|\frac{k_3^+ + \alpha}{k_1^+ + \alpha}\right| |c|^2, \qquad T_{\uparrow\downarrow} = \left|\frac{k_3^- - \alpha}{k_1^+ - \alpha}\right| |d|^2 \qquad [11]$$

Intensity plots of transmission T and reflection R, probabilities as function of E and B, for L = 1.0 is shown in Fig. 8. When z = 0, spin-up reflection is possible at low energy, this is because the normal metal N2 acts as a barrier for the incoming electron. Introducing the potential barrier z, N2-induced spin-up reflection occurs but reduces to zero as the energy increases. Thereafter, a potential barrier-induced spin-up reflection then occurs and keeps increasing to a steady value. During the second stage of spin-up reflection, increasing the energy energizes the reflection process. The opposite occurs during the transmission processes.

ISSN No:-2456-2165

Using the BTK formalism explained in Section II, the difference between $f_{\rightarrow}(E)$ and $f_{\leftarrow}(E)$; the distribution functions at the incident point and reflection point, we have

$$f_{\rightarrow}(E) - f_{\leftarrow}(E) = f_0(E - eV) - \big(f_0(E - eV)(|a(E)|^2 + |b(E)|^2 + |e_3(E)|^2 + |e_4(E)|^2) + f_0(|c(E)|^2 + |d(E)|^2 + |e_1(E)|^2 + |e_2(E)|^2)\big) = \big(f_0(E - eV) - f_0(E)\big)(1 - |a(E)|^2 - |b(E)|^2 - |e_3(E)|^2 - |e_4(E)|^2) \quad [12]$$

Therefore, Eq. (5) becomes

$$G(E) = G_0(1 - |a(E)|^2 - |b(E)|^2 - |e_3(E)|^2 - |e_4(E)|^2) \quad [13]$$

The characteristic plots of the conductance as a function of the energy for L = 0 and L = 1 are shown in Fig. 9. The tunneling conductance G(E) decreases with increasing barrier strength z in both the trivial and non-trivial phases. When L = 1, the tunneling conductance can quickly attain maximum values as the energy of the electron increases; for both trivial and non-trivial phases, unlike when L = 0. We also find that the zero-bias conductance abruptly jumps from G(0) = 0 in the trivial regime to G(0) = 1 in the non-trivial regime.

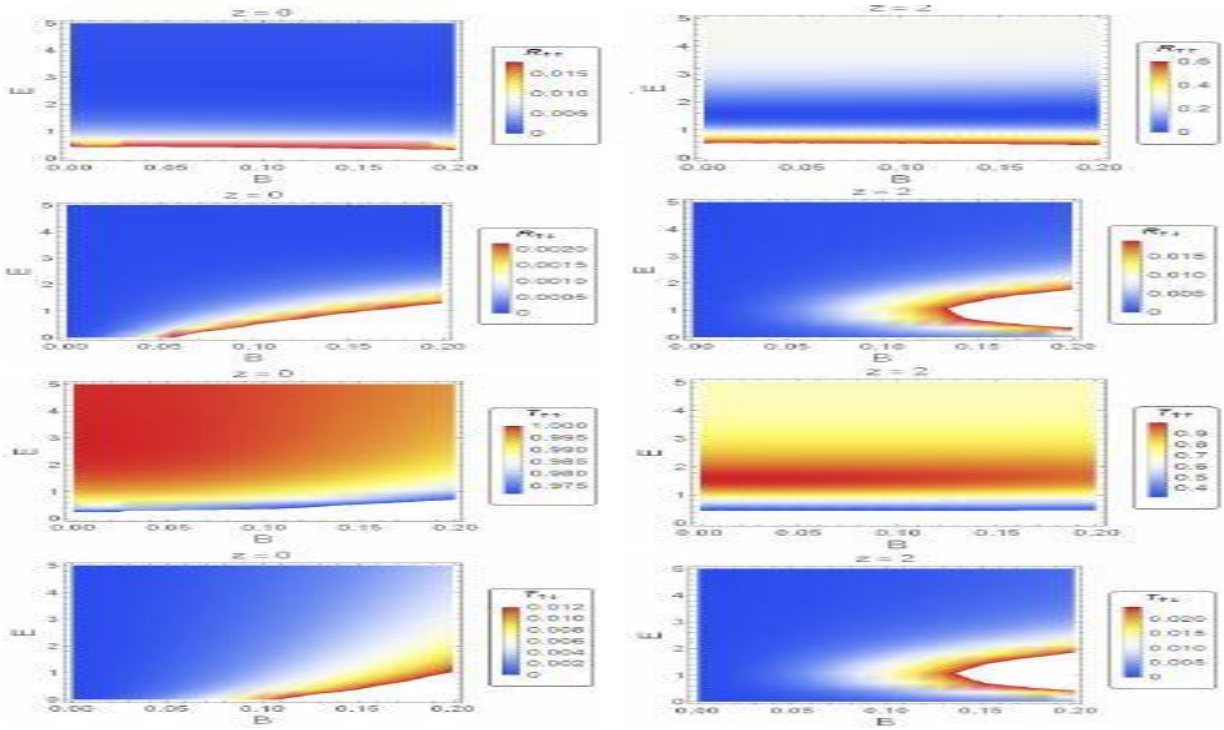

Fig 8 Intensity plots of Transmission (T) and reflection (R) probabilities as function of E and B for fixed z at L = 1.0 for N1-N2-N3 junctions. The potential barrier are z = 0 and 2.0. The other parameters are $\mu_1 = 0.3$, $\mu_2 = 0.5$, $\mu_3 = 0.3$ and $\alpha_R = 0.05$.

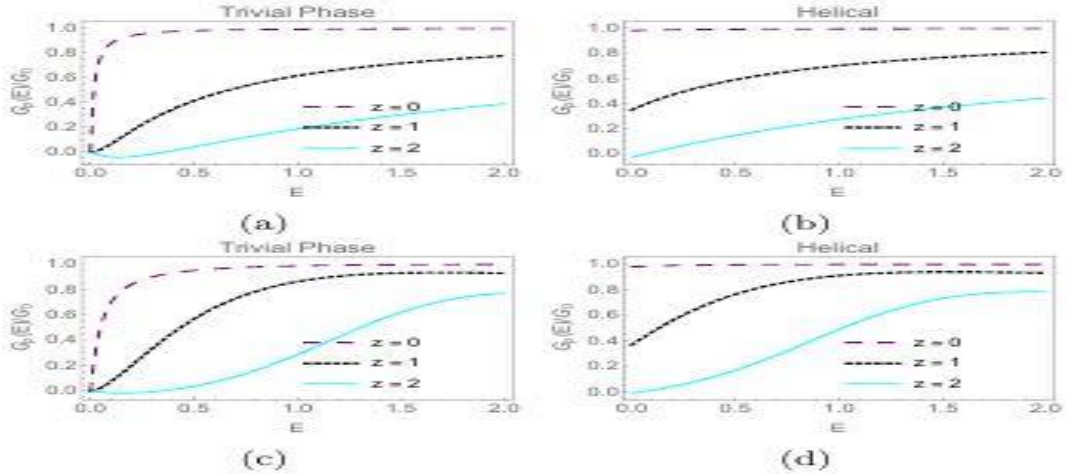

Fig 9 Variation of the Conductance G(E) with Energy E and Barrier Strength z for N1-N2-N3 Junctions. A and C: Trivial Phase: $\mu_1 = 0$, $\mu_2 = 0.2$, $\alpha_R = 0.1$ and B = 0. b and d: Helical: $\mu_1 = 0.4$, $\mu_2 = 0.5$, $\alpha_R = 0.1$ and B = 0.1. Also, We have chosen L = 0 for a and b, and L = 1 for C and D.

IV. CONCLUSION

When two nanowires are coupled together such that one has only SOC and the other have SOC and magnetism, reflection, and transmission of an electron occur at their interface. In the absence of the barrier strength z, reflection does not occur (Although when $\mu_1 < \mu_2$, μ_2 acts as a small barrier, and allows for small reflection at low energy. This reflection becomes insignificant at higher energy), the electron will be maximally transmitted. Transmission of an electron reduces as z increases while reflection increases, but as the energy of the electron increases transmission increases while reflection reduces to minimal.

The tunneling conductance decreases with increasing barrier strength in both trivial and non-trivial phases. In the N1-N2-N3 junctions, when L = 1.0, the tunneling conductance can quickly attain maximum values as the energy of the electron increases in both phases unlike when L = 0. The zero-bias conductance abruptly jumps from G(0) = 0 in the trivial regime to G(0) = 1 in the non-trivial regime. This is unlike what would be obtained in the superconducting state, where the electron can undergo the Andreev reflection, which effectively carries over 2 electrons to a superconductor. As such, a particle with energy E gets completely Andreev reflected, and $G(E)/G_0$ (E) = 2.

ACKNOWLEDGEMENTS

We wish to acknowledge and appreciate the different authors whose articles were used to make this article a reality.

REFERENCES

[1]. Alicea J., Oreg Y., Refael G., von Oppen F., and Fisher M. P. A. (2011). Non-Abelian statistics and topological quantum information processing in 1D wire networks. Nature Physics, vol. 7, pp. 412 - 417.

[2]. Lutchyn, R. M., Sau, J. D. and Das Sarma, S. (2010). Majorana fermions and a topological phase transition in semiconductor-superconductor heterostructures. Phys. Rev. Lett. 105, 077001.

[3]. Oreg Yuval, Refael Gil and von Oppen Felix. (2010). Helical Liquids and Majorana Bound States in Quantum Wires. Physical Review Letters, 105, 177002

[4]. Sela, Eran; Altland, Alexander; Rosch, Achim (2011). Majorana fermions in strongly interacting helical liquids. Physical Review B, 84(8), 085114

[5]. Mourik V., Zuo K., Frolov S. M., Plissard S. R., Bakkers E. P. A. M., and Kouwenhoven L. P. (2012). Signatures of majorana fermions in hybrid superconductor-semiconductor nanowire devices. Science, 336(6084):1003–1007

[6]. Kallaher, R. L.; Heremans, J. J.; Goel, N.; Chung, S. J.; Santos, M. B. (2010). Spin-orbit interaction determined by antilocalization in an InSb quantum well. Physical Review B, 81(7), 075303

[7]. Fadaly, Elham M. T.; Zhang, Hao; Conesa-Boj, Sonia; Car, Diana; Gül, Önder; Plissard, Sébastien Romain; Op het Veld, Roy L. M.; Koelling, Sebastian; Kouwenhoven, Leo P; Bakkers, Erik P.A.M. (2017). Observation of Conductance Quantization in InSb Nanowire Networks. Nano Letters, (), acs.nanolett.7b00797

[8]. Estrada Saldaña, Juan Carlos; Niquet, Yann-Michel; Cleuziou, Jean-Pierre; Lee, Eduardo J. H.; Car, Diana; Plissard, Sébastien R.; Bakkers, Erik P. A. M.; De Franceschi, Silvano (2018). Split-Channel Ballistic Transport in an InSb Nanowire. Nano Letters, (), acs.nanolett.7b03854

[9]. Aseev, Pavel; Wang, Guanzhong; Binci, Luca; Singh, Amrita; Martí-Sánchez, Sara; Botifoll, Marc; Stek, Lieuwe J.; Bordin, Alberto; Watson, John D.; Boekhout, Frenk; Abel, Daniel; Gamble, John; Van Hoogdalem, Kevin; Arbiol, Jordi; Kouwenhoven, Leo; de Lange, Gijs; Caroff, Philippe (2019). Ballistic InSb nanowires and networks via metal-sown selective area growth. Nano Letters, acs.nanolett.9b04265

[10]. Iorio, Andrea; Rocci, Mirko; Bours, Lennart; Carrega, Matteo; Zannier, Valentina; Sorba, Lucia; Roddaro, Stefano; Giazotto, Francesco; Strambini, Elia (2018). Vectorial control of the spin-orbit interaction in suspended InAs nanowires. Nano Letters, (), acs.nanolett.8b02828.

[11]. Badawy, Ghada; Gazibegovic, Sasa; Borsoi, Francesco; Heedt, Sebastian; Wang, Chien-An; Koelling, Sebastian; Verheijen, Marcel A.; Kouwenhoven, Leo; Bakkers, Erik P.A.M. (2019). High Mobility Stemless InSb Nanowires. Nano Letters, (), acs.nanolett.9b00545

[12]. Plissard, Sébastien R.; Slapak, Dorris R.; Verheijen, Marcel A.; Hocevar, Moïra; Immink, George W. G.; van Weperen, Ilse; Nadj-Perge, Stevan; Frolov, Sergey M.; Kouwenhoven, Leo P.; Bakkers, Erik P. A. M. (2012). From InSb Nanowires to Nanocubes: Looking for the Sweet Spot. Nano Letters, 12(4), 1794–1798.

[13]. Liu, Yu; Vaitiekėnas, Saulius; Martí-Sànchez, Sara; Koch, Christian; Hart, Sean; Cui, Zheng; Kanne, Thomas; Khan, Sabbir A.; Tanta, Rawa; Upadhyay, Shivendra; Cachaza, Martin Espiñeira; Marcus, Charles M.; Arbiol, Jordi; Moler, Katherine A.; Krogstrup, Peter (2019). Semiconductor - Ferromagnetic Insulator - Superconductor Nanowires: Stray Field and Exchange Field. Nano Letters, (), acs.nanolett.9b04187.

[14]. [14] Sasaki, Satoshi; Tateno, Kouta; Zhang, Guoqiang; Suominen, Henri; Harada, Yuichi; Saito, Shiro; Fujiwara, Akira; Sogawa, Tetsuomi; Muraki, Koji (2013). Encapsulated gate-all-around InAs nanowire field-effect transistors. Applied Physics Letters, 103(21), 213502

[15]. Burke, A. M.; Carrad, D. J.; Gluschke, J. G.; Storm, K.; Fahlvik Svensson, S.; Linke, H.; Samuelson, L.; Micolich, A. P. (2015). InAs Nanowire Transistors with Multiple, Independent Wrap-Gate Segments. Nano Letters, 15(5), 2836–2843.

[16]. Yin Yiheng; Zhaofu Zhang; Hongxia Zhong;Chen Shao; Xuhao Wan; Can Zhang; John Robertson; Yuzheng Guo; (2021). Tellurium Nanowire Gate-All-Around MOSFETs for Sub-5 nm Applications . ACS Applied Materials and amp; Interfaces, doi:10.1021/acsami.0c18767
[17]. Braunecker, Bernd; Japaridze, George I.; Klinovaja, Jelena; Loss, Daniel (2010). Spin-selective Peierls transition in interacting one-dimensional conductors with spin-orbit interaction. Physical Review B, 82(4), 045127
[18]. Stoudenmire, E. M.; Alicea, Jason; Starykh, Oleg A.; Fisher, Matthew P.A. (2011). Interaction effects in topological superconducting wires supporting Majorana fermions. Physical Review B, 84(1), 014503.
[19]. Schmidt, Thomas L. (2013). Finite-temperature conductance of interacting quantum wires with Rashba spin-orbit coupling. Physical Review B, 88(23), 235429
[20]. Schmidt, Thomas L. and Pedder, Christopher J. (2016). Helical gaps in interacting Rashba wires at low electron densities. Physical Review B, 94(12), 125420.
[21]. Kane, C. L.; Mukhopadhyay, Ranjan; Lubensky, T. C. (2002). Fractional Quantum Hall Effect in an Array of Quantum Wires. Physical Review Letters, 88(3), 036401.
[22]. Teo, Jeffrey C. Y. and Kane, C. L. (2014). From Luttinger liquid to non-Abelian quantum Hall states. Physical Review B, 89(8), 085101.
[23]. Scheller, C. P., Liu, T. M., Barak, G., Yacoby, A., Pfeiffer, L. N., West, K. W., and Zumbuhl, D. M. (2014). Possible Evidence for Helical Nuclear Spin Order in GaAs Quantum Wires. Physical Review Letters, 112 (6), 066801.
[24]. Cayao, Jorge; Prada, Elsa; San-Jose, Pablo; Aguado, Ramón (2015). SNS junctions in nanowires with spin-orbit coupling: Role of confinement and helicity on the subgap spectrum. Physical Review B, 91(2), 024514.
[25]. Blonder, G.E., Tinkham, M. and Klapwijk, T.M. (1982). Transition from metallic to tunneling regimes in superconducting microconstrictions: Excess current, charge imbalance, and supercurrent conversion. Phys. Rev. B 25, 4515.
[26]. Sharvin, Yu. V. (1965). A Possible Method for Studying Fermi Surfaces. Soviet Physics JETP, Vol. 21, p.655.
[27]. Lukic, Vladimir. (2002). Conductance of superconductor -normal metal contact junction beyond quasiclassical approximation. University of Illinois at Urbana-Champaign ProQuest Dissertations Publishing, 3202136.
[28]. Cayao Jorge. (2016). Hybrid superconductor-semiconductor nanowire junctions as usefulplatforms to study Majorana bound states. arXiv:1703.07630v1.
[29]. Pedder, Christopher J.; Meng, Tobias; Tiwari, Rakesh P.; Schmidt, Thomas L. (2016). Dynamic response functions and helical gaps in interacting Rashba nanowires with and without magnetic fields. Physical Review B, 94(24), 245414

APPENDIX A: NANOWIRES WITHOUT RASHBA SPIN-ORBIT COUPLING AND MAGNETIC FIELD

Consider two nanowires, N1 and N2, coupled together without spin-orbit coupling and magnetic field. The Hamiltonian for the system is given by

$$H_0 = \frac{p^2}{2m} - \mu_i \qquad [A1]$$

p is the momentum, m is the effective electron mass and μ is the chemical potential, and "i" represents the left or right region. The Hamiltonian in the left region is given by $H_0^1 = \frac{p^2}{2m} - \mu_1$.

The Schrödinger equation for this region is $\frac{d^2\psi}{dx^2} + k_1^2\psi = 0$, with eigenvalue $E_1 = \frac{\hbar^2 k_1^2}{2m} - \mu_1$, where the wave number $k_1 = \pm\sqrt{\frac{2m}{\hbar^2}(E_1 + \mu_1)}$. Fig. 10 shows the energy versus momentum dispersion for a free electron that consists of a single parabola. At k = 0, the electron has the minimum energy, $E_1 = -\mu_1$. As μ_1 increases, the energy reduces to the point where there are no Fermi points.

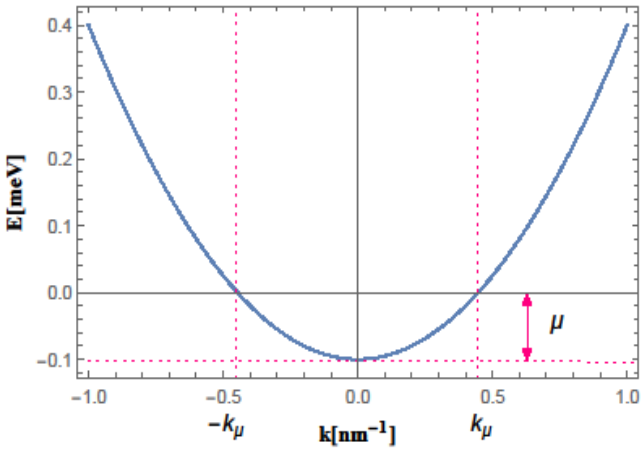

Fig. 10 Energy Spectrum for the Left/Right Region

The Schrödinger equation has the solution of the form

$$\psi(x) = Fe^{-ik_1x} + Ge^{ik_1x}. \qquad [A2]$$

If we consider a particle moving to the right, the coefficient $F = 0$. The eigenfunction in the left region is therefore given as, $\psi_k^1(x) = e^{ik_1x}$, where $G = 1$for a free particle. The wavevector has an imaginary term when$E_1 + \mu_1 < 0$. The corresponding wavefunction is given by $\psi_k^1(x) = e^{\mp\sqrt{t_1}x}$, where$t_1 = \left|\frac{2m}{\hbar^2}(E_1 + \mu_1)\right|$.

Let's consider a particle traveling to the left, the Hamiltonian in the right region reads $H_0^2 = \frac{p^2}{2m} - \mu_2$. The Schrödinger equation (SE) reads $\frac{d^2\psi}{dx^2} + k_2^2\psi = 0$ and has the solution of the form $\psi(x) = Ae^{-ik_2x} + Be^{ik_2x}$. Also, a free particle traveling to the left has the coefficient $A = 0$. The eigenvector in the right region is therefore given as $\psi_k^2(x) = e^{ik_2x}(x > 0)$. If we consider the scattering states for this system, the SE for $x < 0$ reads

$$\frac{d^2\psi}{dx^2} + k^2\psi = 0. \quad [A3]$$

The general solution for Eq. (A3) in the left region due to an incident electron is given by

$$\psi_1(x) = e^{ik_1x} + re^{-ik_1x}. \quad [A4]$$

The first term represents the incident wave, the second term represents the reflected wave and r is the reflection coefficient. Similarly, in the right region, $x > 0$, the transmitted wave in the right region is given by

$$\psi_2(x) = te^{ik_2x}, \quad [A5]$$

where t is the transmission coefficient. The continuity of $\psi(x)$ at $x = 0$ requires that

$$\psi(x < 0) = \psi(x > 0). \quad [A6]$$

Also, the discontinuity of the derivative at$x = 0$ is given by

$$\Delta\left(\frac{d\psi(x)}{dx}\right) = Z\psi(x = 0), \quad [A7]$$

Where $Z = \frac{2m}{\hbar^2}V$. Using equations (A6) and (A7), the reflection probability was obtained as

$$R = \frac{(k_1-k_2)^2+Z^2}{(k_1+k_2)^2+Z^2} \quad [A8]$$

And the transmission probability as

$$T = \frac{4k_1k_2}{(k_1+k_2)^2+Z^2}. \quad [A9]$$

APPENDIX B: SCATTERING STATES

We considered two nanowires N1 and N2, coupled together to produce a junction. N1 is a Rashba nanowire and N2 is a Rashba nanowire subjected to an external magnetic field. The wavefunction describing the scattering states at the interface between them is

$$\begin{aligned}\Psi(x) &= \phi_1^+e^{ik_1^+x} + a\phi_1^+e^{-ik_1^+x} + b\phi_1^-e^{-ik_1^-x}x < 0\\ \Psi(x) &= c\phi_2^+e^{ik_2^+x} + d\phi_2^-e^{ik_2^-x} \qquad x > 0\end{aligned} \quad [B1]$$

Where

$$\begin{aligned}&\phi_1^+ = \frac{1}{\sqrt{2}}\binom{i}{1}, \phi_1^- = \frac{1}{\sqrt{2}}\binom{-i}{1}, \phi_2^+ = \frac{1}{\sqrt{2}}\binom{\gamma}{1}, \phi_2^- = \frac{1}{\sqrt{2}}\binom{-\gamma}{1}\\ &k_1^+ = -k_{so} \pm \sqrt{k_{so}^2 + k_E^2 + k_\mu^2}, k_1^- = k_{so} \pm \sqrt{k_{so}^2 + k_E^2 + k_\mu^2},\\ &k_2^+ = -\sqrt{2k_{so}^2 + k_\mu^2 + k_E^2 + \sqrt{(k_\mu^2 + 2k_{so}^2)^2 - k_\mu^4 + k_Z^4 + 4k_E^2k_{so}^2}},\\ &k_2^- = \sqrt{2k_{so}^2 + k_\mu^2 + k_E^2 + \sqrt{(k_\mu^2 + 2k_{so}^2)^2 - k_\mu^4 + k_Z^4 + 4k_E^2k_{so}^2}}.\end{aligned} \quad [B2]$$

The boundary conditions were obtained by introducing a delta potential $U\delta(x)$ in the Hamiltonian of the system,

$$H_0 = \left(\frac{p^2}{2m} - \mu_0\right)\sigma_0 - \frac{\alpha_R}{\hbar}p\sigma_y + B\sigma_x + U\delta(x)\sigma_x \quad [B3]$$

Then, the integration $H_0(x)\Psi(x) = E\Psi(x)$ gives $\left(\frac{d\Psi(x)}{dx}\Big|_{\varepsilon^+} - \frac{d\Psi(x)}{dx}\Big|_{\varepsilon^-}\right)\sigma_x = \frac{2m}{\hbar^2}(U\sigma_x - i\alpha_R\sigma_y)\Psi(x = 0),$ [B4]

where $Z = \frac{2m}{\hbar^2}U$. Eq. (B4) represents the discontinuity of the derivative at x = 0. Integrating Eq. (B4) around x = 0, we have

$$\Psi(x < 0) = \Psi(x > 0), \quad [B5]$$

which is the continuity of the wavefunction at x = 0. Using the boundary conditions of Eqs. (B4) and (B5), the coefficients are given by

$$\begin{aligned}&a = -\frac{P}{Q_1}, b = -\frac{2ik_1^+(k_2^+-k_2^-)(1+\gamma^2)}{iQ_1},\\ &c = \frac{4k_1^+(i+\gamma)(k_1^-+k_2^-+i(Z-\alpha))}{iQ_1}, d = \frac{4k_1^+(-i+\gamma)(k_1^-+k_2^++i(Z-\alpha))}{iQ_1}.\end{aligned} \quad [B6]$$

Where

$$\begin{aligned}P &= 4\gamma(k_2^+ + i(Z-\alpha))(-ik_2^- + Z - \alpha)\\ &-k_1^-(-k_2^-(-i+\gamma^2) + 4\gamma(-Z+\alpha)) + k_1^+(-i+\gamma)^2\\ &+k_2^-(i+\gamma)^2 + 4\gamma(ik_1^- - Z + \alpha),\\ Q_1 &= k_1^+(k_2^+(-i+\gamma)^2 - k_2^-(i+\gamma)^2\\ &+ 4\gamma(-ik_1^- + Z - \alpha))\\ &+4\gamma(k_2^+ + i(Z-\alpha))(-ik_2^- + Z - \alpha)\\ &-k_1^-(-k_2^-(-i+\gamma)^2 + k_2^+(i+\gamma)^2 + 4\gamma(-Z+\alpha)).\end{aligned} \quad [B7]$$